

Article

# The Promoting Effect of Ce on the Performance of Au/Ce<sub>x</sub>Zr<sub>1-x</sub>O<sub>2</sub> for $\gamma$ -Valerolactone Production from Biomass-Based Levulinic Acid and Formic Acid

Xiaoling Li, Jianmei Li \*, Xudong Liu, Qi Tian and Changwei Hu \*

Key Laboratory of Green Chemistry and Technology, Ministry of Education, College of Chemistry, Sichuan University, Chengdu 610064, China; lingxiaoli2015@163.com (X.L.); liuxudong621@163.com (X.L.); tqinvoker@sohu.com (Q.T.)

\* Correspondence: lijianmei@scu.edu.cn (J.L.); changwei.hu@scu.edu.cn (C.H.); Tel./Fax: +86-28-8541-5608 (J.L.); +86-28-8541-1105 (C.H.)

Received: 28 April 2018; Accepted: 2 June 2018; Published: 7 June 2018



**Abstract:** The production of  $\gamma$ -valerolactone (GVL) directly from biomass-based levulinic acid (LA) and formic acid (FA) without extra hydrogen source is attractive but challenging, due to the requirement of a highly active and stable catalyst. In present work, Au/Ce<sub>x</sub>Zr<sub>1-x</sub>O<sub>2</sub> with various Ce/Zr ratios were prepared as the catalyst for GVL production from LA with the equivalent molar FA, and characterized by XRD, Raman-spectra, BET, NH<sub>3</sub>-TPD, TEM and XPS. It was found that the doped Ce in Au/Ce<sub>x</sub>Zr<sub>1-x</sub>O<sub>2</sub> catalyst could improve the reduction of Au<sup>3+</sup> to metallic Au<sup>0</sup>, and also promoted the dispersion of Au<sup>0</sup>, yielding uniform Au<sup>0</sup> nanoparticles with a small average particle size of about 2.4 nm, thus enhancing both the decomposition of FA to CO-free H<sub>2</sub> and the hydrogenation of LA. Meanwhile, a certain amount of doped Ce ( $x \leq 0.4$ ) could facilitate the formation of tetragonal phase (the most desired structure on LA conversion to GVL), and increase the amount of weak and medium-strength acidic sites of catalyst, thereby promoting the dehydration reaction of the intermediate derived from LA hydrogenation. Au/Ce<sub>0.4</sub>Zr<sub>0.6</sub>O<sub>2</sub> catalyst exhibited the best catalytic activity, achieving 90.8% of LA conversion and 83.5% of GVL yield (TON = 2047.8), with good recyclability, and the activity showed no obvious change after 5 runs.

**Keywords:** levulinic acid; formic acid;  $\gamma$ -valerolactone; Au/Ce<sub>x</sub>Zr<sub>1-x</sub>O<sub>2</sub>

## 1. Introduction

With increasing attention on the production of renewable platform chemicals from biomass, more research has been focused on  $\gamma$ -valerolactone (GVL) production. GVL is considered as one of the most important platform chemicals derived from biomass. GVL can be used as a green solvent in many reactions, including some organic reactions and biomass conversion. GVL can be also used as an additive in food, liquid fuels and perfumes [1,2]. It is found that the gasoline with GVL as fuel additive shows similar fuel properties to that with ethanol as an additive. GVL is a precursor to produce gasoline, diesel fuels and other valuable chemicals such as ionic liquid, methyl pentenoate, 1,4-pentanediol, and polymers [3–5]. In addition, GVL is stable under neutral conditions, and therefore is a safe material for industrial applications [6].

Levulinic acid (LA) can be directly produced from the conversion of raw biomass, and is commonly employed as feedstock to produce GVL with a diverse hydrogen source. Molecular H<sub>2</sub> with high pressure is usually employed as the hydrogen source. However, from both the economic and engineering point of view, this process will arguably be less sustainable, as the worldwide H<sub>2</sub> is produced mainly by the steam reforming of fossil carbon [7–9]. Alcohols, such as ethanol, isopropyl alcohol and butanol, are also employed as the hydrogen source in the process of catalytic

transfer hydrogenation (CTH) [10–12]. Formic acid (FA) is another potential hydrogen source for GVL synthesis, as it shows higher energy density and is easier to be stored and transferred. Formic acid can be produced directly from raw biomass in the acid-catalyzed dehydration process of carbohydrates for levulinic acid production. Actually, the FA amount is a little higher than that of LA, due to the presence of side effects, thus guaranteeing the abundant FA that can be used as an in situ hydrogen source for LA hydroxylation to GVL. In addition, the stream of LA production from biomass conversion contains a high water content (typically more than 70%). Therefore, directly using FA as a hydrogen source and H<sub>2</sub>O as a solvent would avoid the addition of an extra hydrogen source and simplify the purification of LA, and therefore is a more sustainable method.

In the process of GVL production directly from biomass-based LA and FA, the catalyst plays a crucial role in LA conversion and GVL yield [13]. This is especially the case when FA is employed as the hydrogen source in the aqueous solution with high acidity, acid-resistant and stable catalysts in the acidic aqueous solution, as well as the high activity for LA hydrogenation and appropriate acidity for the lactonization to form GVL, are therefore highly demanded. Additionally, the developed catalysts must show high selectivity for the decomposition of FA to H<sub>2</sub> rather than to CO in situ. Although homogeneous catalysts, including Ru(acac)<sub>3</sub>/P(n-Oct)<sub>3</sub>, RuCl<sub>2</sub>(PPh<sub>3</sub>)<sub>3</sub> and Ru(acac)<sub>3</sub>/PBu<sub>3</sub> catalyst [14,15], show high efficiency for LA hydrogenation to GVL when FA is used as the hydrogen source, homogeneous systems are arguably not suitable to target GVL separation, owing to the difficult separation of GVL [16]. Heterogeneous catalysts have attracted more attentions for GVL production. Among the developed heterogeneous catalysts, noble metal (e.g., Ru, Pt, Pd, Rh, Ir and Au) nanoparticles exhibit good performances [8,17–21]. In particular, the Ru catalyst is noticeably the most active. However, recycling experiments indicate that these catalysts are not stable [22,23]. The activity and recyclability of supported catalyst sharply decrease due to the leaching of supported metal in acidic solution. Recently, the use of supported gold nanoparticles (NPs) or clusters for GVL production is an area of growing interest, because of its unique efficiency for formic acid decomposition to CO-free H<sub>2</sub> [24], thereby enabling the efficient reduction of LA without the addition of external H<sub>2</sub> [1,11,25]. In addition to different metal species, the support material can give a significant contribution to the catalytic activity and GVL selectivity, due to their different types and the amount of acidic sites, as well as the interaction with the supported metal [26,27]. For example, Ruppert et al. show that the phases and morphology of titania support strongly influence the physicochemical property of the prepared Pt and Ru catalysts and the efficiency for GVL production from levulinic acid in different ways [28]. Moreover, it is found that the support could also affect the decomposition of formic acid [24,29,30]. Of screening the references, TiO<sub>2</sub>, ZrO<sub>2</sub>, Al<sub>2</sub>O<sub>3</sub>, SiO<sub>2</sub>, CeO<sub>2</sub>, MgO and activated carbon are commonly employed as the supports of the catalyst for GVL production, where zirconia-supported catalysts have shown much better efficiency and stability than others [31,32]. Ftouni et al. indicate that ZrO<sub>2</sub> support shows better efficiency for the dispersion and reduction of metal Ru than TiO<sub>2</sub>, due to the detrimental strong interaction between metal and support, and all catalysts exhibit high efficiency for GVL production. However, only Ru/ZrO<sub>2</sub> catalyst shows good recyclability [33]. Du et al. also report that Au/ZrO<sub>2</sub> shows much higher activity than Au/TiO<sub>2</sub> for LA hydrogenation to GVL, whereas Au/SiO<sub>2</sub> and Au/C are less active [1]. Therefore, it is of particular importance to reveal the performance of support on the catalytic efficiency of the catalyst [34,35].

In our previous work [36], we find that Pt/C is effective for FA decomposition to H<sub>2</sub> in situ with high selectivity, thus promoting the GVL yield. However, excessive formic acid (three times over LA molar amount) is needed to achieve the highest TON value, which suggest that the hydrogen source that accompanied LA formation is not enough to produce GVL, thus inhibiting further application in practice. As we know, the Ce-Zr solid solution is widely employed to prepare a three-way catalyst, while it is rarely used for hydrogenation reactions. This present work aiming at deeply understanding the effect of support and further improving its performance for LA hydrogenation to form GVL with equivalent molar FA, Au nanoparticles supported on Ce<sub>x</sub>Zr<sub>1-x</sub>O<sub>2</sub> solid solution are prepared as the

catalyst. The performance of doped Ce on the morphology and activity of catalyst on the production of GVL is investigated.

## 2. Results and Discussion

### 2.1. Catalyst Characterization

The XRD patterns (Figure 1A) show that both tetragonal (*t*) and monoclinic (*m*) phases are present in pure  $ZrO_2$ , although the monoclinic phase is more thermodynamically stable than the metastable tetragonal phase. This is possibly caused by the small particle size (11 nm) of prepared  $ZrO_2$  support, which can favor the stabilization of the tetragonal phase. In the case of  $CeO_2$ , three characteristic peaks assigning to (111), (200) and (220) of cubic phase (ref. JCPDS card 34-394) are observed. For the sample of  $Ce_xZr_{1-x}O_2$  solid solution, no peaks are detected for pure  $ZrO_2$  or  $CeO_2$  species, indicating the absence of phase separation or surface segregation and proving the formation of  $Ce_xZr_{1-x}O_2$  solid solutions. Based on the Scherrer equation,  $Ce_xZr_{1-x}O_2$  shows a smaller average crystallite size (7–9 nm) than both pure  $CeO_2$  (14 nm) and pure  $ZrO_2$  (11 nm). This is probably ascribed to the fact that the presence of  $CeO_2$  in supports decelerates the crystallite growth of crystal phase in  $ZrO_2$ , which can also lead to an increase of lattice defects [37]. The Ce/Zr ratio greatly affects the crystalline structure of  $Ce_xZr_{1-x}O_2$ . In the case of  $Ce_{0.1}Zr_{0.9}O_2$ ,  $Ce_{0.2}Zr_{0.8}O_2$  and  $Ce_{0.3}Zr_{0.7}O_2$ , a pure tetragonal phase is observed. Continuously increasing  $CeO_2$  content to 40% and 50%, the XRD patterns are broadened and shift gradually to lower values of  $2\theta$ , owing to the substitution of  $Zr^{4+}$  (ionic radius 0.84 Å) with the bigger  $Ce^{4+}$  ion (0.96 Å) in the lattice which results in the changes in the lattice parameters [38]. Consequently, a cubic phase gradually appears especially at  $x = 0.5$ , giving a mixture of tetragonal and cubic phases. When Au is supported on  $Ce_4Zr_{0.6}O_2$  solid solution, the similar crystalline structure is observed (Figure 1B). However, the diffraction peaks of crystalline Au could not be observed with an Au loading ranging from 0.2 to 1.0 wt %, which indicates that the Au particle size on these catalysts is very small. Further increasing Au loading from 1.4 to 2.2 wt %, a very small amount of crystalline gold is observed as demonstrated by the weak peak at  $2\theta = 38.2^\circ$ .

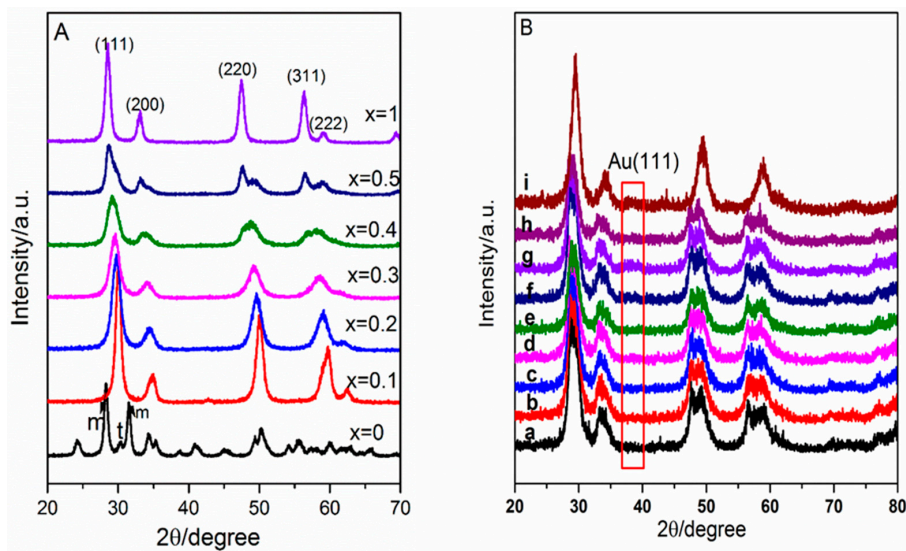


**Figure 1.** X-ray diffraction patterns of (A):  $Ce_xZr_{1-x}O_2$  support; (B): catalysts with different Au loadings and the used catalyst (a 0.2 wt %, b 0.3 wt %, c 0.6 wt %, d 0.8 wt %, e 1 wt %, f 1.4 wt %, g 2 wt %, h 2.2 wt %, i the used catalyst after five runs).

The  $N_2$  adsorption-desorption isotherms of catalysts are plotted in Figure S1. The curves of  $Ce_xZr_{1-x}O_2$  solid solution display a type H2 hysteresis loop, where the pore size distribution is relatively uniform in the range of 2–10 nm. In addition, the relative pressure in the isotherms shows a

very narrow range, suggesting that the adsorption is very low in the micropore range. The distribution of pore size is calculated by BJH model [39], which shows that  $Ce_xZr_{1-x}O_2$  solid solution with different Ce loading presents quite a narrow distribution of mesopore diameter between 2.9 and 3.7 nm (Table S1). However, H4 hysteresis loop is observed in the case of pure  $CeO_2$ , where the pore structure is in 2–100 nm and is not regular. It indicates that there is a certain amount of large pore in pure  $CeO_2$ , and the distribution of the hole is very uneven.

Raman spectra of  $ZrO_2$ ,  $CeO_2$ , and  $Ce_xZr_{1-x}O_2$  solid solution are collected over the range of 140–800  $cm^{-1}$  (Figure 2), in order to assign the actual phases of samples. A complex spectrum (up to 18 vibration modes) is collected for  $ZrO_2$ , attributing to the overlap of tetragonal and monoclinic phases. This confirms the result of XRD that both monoclinic and tetragonal phases are present in pure  $ZrO_2$ . For the sample of  $CeO_2$ , only one  $F_{2g}$  mode centered at around 450  $cm^{-1}$  is Raman-active, implying the presence of cubic phase. In the case of  $Ce_xZr_{1-x}O_2$  ( $x = 0.1, 0.2, 0.3$ ) solid solution, the Raman spectra become simpler, and five Raman bands located at 146, 253, 300, 447, 625  $cm^{-1}$  and one shoulder at 560  $cm^{-1}$  are observed, indicating the presence of tetragonal phase [40]. For the samples with high Ce content especially  $x = 0.5$ , the peaks at 253 and 560  $cm^{-1}$  decrease gradually. In combination with the significant strengthening of the peak at 450  $cm^{-1}$ , it can be speculated that both cubic and tetragonal phases are present in  $Ce_{0.4}Zr_{0.6}O_2$  and  $Ce_{0.5}Zr_{0.5}O_2$  solid solutions. This result is well in agreement with that of XRD. Thus, it is considered that a certain amount of doped Ce can facilitate the formation of the support with a tetragonal phase.

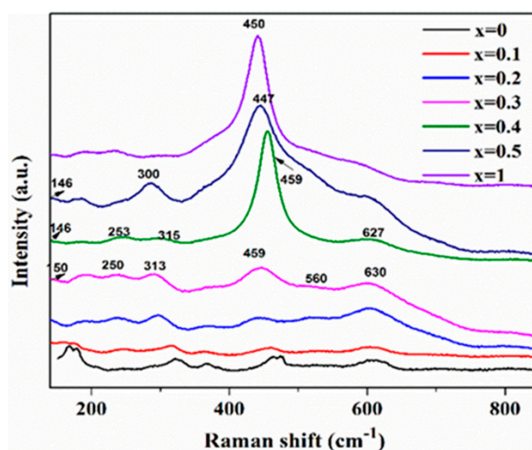


Figure 2. Raman spectra of  $Ce_xZr_{1-x}O_2$ .

We used  $NH_3$ -TPD analysis to probe the acidity of the support (Figure 3). The peaks in the low-temperature (LT) region below 400 °C represent the release of  $NH_3$  from weak (<200 °C) and moderate (200–400 °C) acidic sites, whereas the peaks in high-temperature (HT, >400 °C) region belong to the  $NH_3$  desorption from strong acidic sites [41]. To investigate the effect of Ce/Zr ratio on the distribution of different acidic sites, peak fitting is performed by dividing the spectrum into four peaks. Gaussian deconvolution method is used to deconvolute the  $NH_3$ -TPD profiles in this work. Considering that the pretreatment conditions of catalyst samples were consistent, the obvious difference in  $NH_3$ -TPD diagram above 500 °C was assumed to be caused by the desorption of  $NH_3$ , although the pretreatment temperature of the samples is set to be 500 °C [42]. The total acid amount of  $Ce_xZr_{1-x}O_2$  is higher than that of both pure  $ZrO_2$  and  $CeO_2$ , implying that the introduction of Ce into  $ZrO_2$  can improve the acidity of  $Ce_xZr_{1-x}O_2$  solid solution. With increasing Ce content, the total acid amount gradually increases and gets the maximum (1.34  $mmol \cdot g^{-1}$ ) at  $x = 0.4$ . However, a higher Ce content than 40% leads to the decrease of the total amount of acidic sites. Moreover, it is demonstrated that a certain amount of doped Ce predominantly increases the weak and moderate acidic sites. This is possibly due to the formation of Zr-O-Ce bond [43].

A careful TEM analysis is carried out on 2 wt % Au/ZrO<sub>2</sub>, Au/CeO<sub>2</sub> and Au/Ce<sub>0.4</sub>Zr<sub>0.6</sub>O<sub>2</sub> to reveal the effect of doped Ce on the gold dispersion, and the results are summarized in Figure 4. Based on the TPR profile of Au/Ce<sub>0.4</sub>Zr<sub>0.6</sub>O<sub>2</sub>, the catalyst is reduced at 350 °C, in the atmosphere of 5% H<sub>2</sub>/Ar for 2 h. The color of the precursor (Ce<sub>x</sub>Zr<sub>1-x</sub>O<sub>2</sub>) is yellow. When the catalyst is reduced at 350 °C for 2 h, the catalyst becomes purple. For morphology analysis, after reduction, roundish gold nanoparticles are obviously observed and well-distributed over the support. Au particles supported on ZrO<sub>2</sub> (Figure 4a) has a size ranging from 1.7 to 4.2 nm with a mean size of around 3.2 nm. After doping Ce into the support, Au/Ce<sub>0.4</sub>Zr<sub>0.6</sub>O<sub>2</sub> shows smaller Au size in the range of 1.2–3.5 nm with a mean size of 2.4 nm (Figure 4b). Au/CeO<sub>2</sub> (Figure 4c) exhibits narrower Au size distribution (2.0–3.8 nm) but larger particle size than that of Au/Ce<sub>0.4</sub>Zr<sub>0.6</sub>O<sub>2</sub>, indicating the promotion of doped Ce on the dispersion of Au on the supports. This result is well consistent with that reported by B. Harrison, which points out that CeO<sub>2</sub> stabilizes the metal dispersion on alumina support [44].

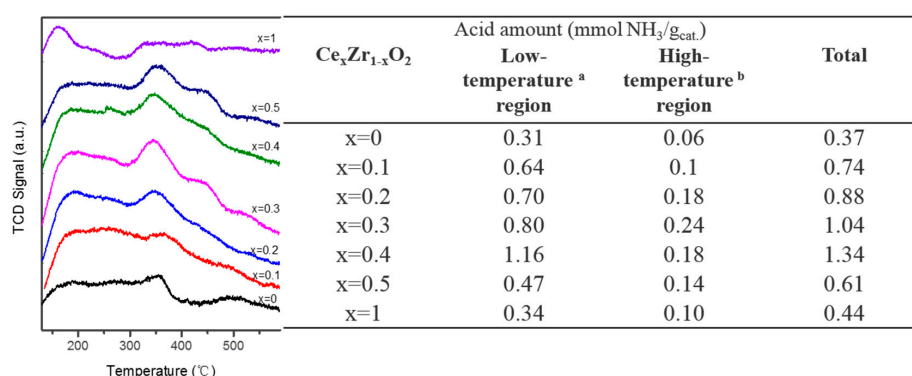


Figure 3. The NH<sub>3</sub>-TPD patterns and the calculated acid amounts of Ce<sub>x</sub>Zr<sub>1-x</sub>O<sub>2</sub>.

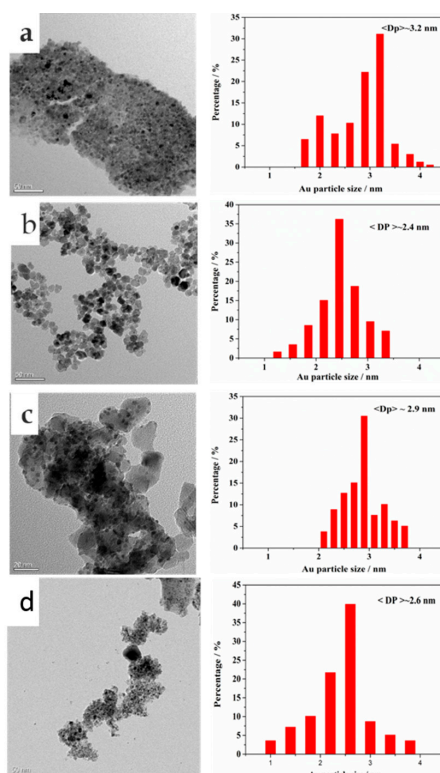


Figure 4. TEM images and the distribution of gold particle size of catalysts (a) Au/ZrO<sub>2</sub>; (b) Au/Ce<sub>0.4</sub>Zr<sub>0.6</sub>O<sub>2</sub>; (c) Au/CeO<sub>2</sub>; (d) the reused catalyst after five runs.

The surface composition of reduced Au/Ce<sub>x</sub>Zr<sub>1-x</sub>O<sub>2</sub> catalyst is analyzed by XPS (Figure 5, Figure S2). The composition of Au/Ce<sub>x</sub>Zr<sub>1-x</sub>O<sub>2</sub> catalyst in the bulk is analyzed by XRF. As for the atomic ratio of Ce/Zr, it is noted that the ratio of Ce to Zr in the bulk of catalyst ((Ce/Zr)<sub>bulk</sub>) is close to that in the surface ((Ce/Zr)<sub>XPS</sub>), except for Au/Ce<sub>0.5</sub>Zr<sub>0.5</sub>O<sub>2</sub> (Table 1). This suggests that the composition of solid solutions on the surface is similar to that in the bulk, without obvious surface aggregation. Compared to that in the bulk, the Ce/Zr ratio on the surface of Au/Ce<sub>0.5</sub>Zr<sub>0.5</sub>O<sub>2</sub> is a little higher, indicating surface enrichment in cerium when Ce content increases to 50%. The atomic Au/(Ce+Zr)<sub>XPS</sub> ratios gradually increase with cerium content, and obtain the maximum at x = 0.4, indicating the better dispersion of gold with increasing Ce loading. This further confirms the XRD (Figure 1B) and TEM (Figure 4) results, and proves that CeO<sub>2</sub> can promote the dispersion of Au on the supports [43]. However, when the cerium content in the support is higher than 50% (x ≥ 0.5), a decrease in Au dispersion is observed.

**Table 1.** XPS characterization of Au/Ce<sub>x</sub>Zr<sub>1-x</sub>O<sub>2</sub> catalysts.

Catalyst	Percentage (%)		(Ce/Zr) <sub>bulk</sub> <sup>a</sup>	(Ce/Zr) <sub>XPS</sub>	Au/(Ce + Zr) <sub>XPS</sub>
	Au <sup>n+</sup>	Au <sup>0</sup>			
Au/ZrO <sub>2</sub>	32.9	67.1	—	—	0.007
Au/Ce <sub>0.1</sub> Zr <sub>0.9</sub> O <sub>2</sub>	23.7	76.3	0.07	0.11	0.010
Au/Ce <sub>0.2</sub> Zr <sub>0.8</sub> O <sub>2</sub>	27.7	72.3	0.19	0.24	0.009
Au/Ce <sub>0.3</sub> Zr <sub>0.7</sub> O <sub>2</sub>	11.1	88.9	0.37	0.47	0.020
Au/Ce <sub>0.4</sub> Zr <sub>0.6</sub> O <sub>2</sub>	10.6	89.4	0.45	0.53	0.022
Au/Ce <sub>0.5</sub> Zr <sub>0.5</sub> O <sub>2</sub>	20.9	79.3	0.67	0.88	0.011
Au/CeO <sub>2</sub>	18.4	81.6	—	—	0.008

<sup>a</sup> Results obtained from XRF measurements.

The Zr 3d<sub>5/2</sub> binding energy at around 182.2 eV remains unchanged for all the catalysts. This result is consistent with the result of Eder et al., where it is demonstrated that higher temperature than 973 K is required for ZrO<sub>2</sub> reduction [45]. As for the Au(4f) spectrum, two peaks at 84.0 and 87.7 eV are observed, indicating the existence of metallic Au<sup>0</sup> (Figure 5a). The additional shoulders at around 85.9 and 89.6 eV are assigned to gold species with positive charge (Au<sup>+</sup> or Au<sup>3+</sup>, defined as Au<sup>n+</sup>) [40]. With increasing Ce content, a slight shift of Au<sup>0</sup> signal towards low binding energy is observed, demonstrating the electron transfer from support Ce<sub>x</sub>Zr<sub>1-x</sub>O<sub>2</sub> to Au [46]. The relative concentration of metallic Au<sup>0</sup> on Au/Ce<sub>x</sub>Zr<sub>1-x</sub>O<sub>2</sub> is much higher than that in the Au/ZrO<sub>2</sub> catalyst, demonstrating that the doped Ce can favor the reduction of Au<sup>n+</sup> to Au<sup>0</sup>. This can be further proved by the obvious decrease of reduction temperature of Au<sup>3+</sup> after doping Ce. When the content of Ce is up to 40%, the relative concentration of metallic Au<sup>0</sup> reaches up to the highest value (89.4%). It is worthy of noticing that Ce<sup>3+</sup> is observed in the catalysts after calcination, indicating the transition of Ce<sup>4+</sup> to Ce<sup>3+</sup> in the calcination process at high temperature (Figure S2 and Table S2) [47]. The percentage of Ce<sup>3+</sup> shows no obvious change when Au<sup>3+</sup> is loaded on the support by the simple deposition-precipitation (DP) method without further calcination. However, the intensities of Ce<sup>3+</sup> characteristic peaks obviously increase after reduction in most of the cases, indicating the further reduction of Ce<sup>4+</sup> in close to the metal. Especially for Au/Ce<sub>0.4</sub>Zr<sub>0.6</sub>O<sub>2</sub> catalyst, the highest increment of Ce<sup>3+</sup> percentage is observed. This can be ascribed to two possible reasons. One is related to the easy reduction of Au<sup>3+</sup> with the introduction of Ce, which can lead to the simultaneous reduction of Ce<sup>4+</sup>. The other involves that the reduced Au can further adsorb H<sub>2</sub> and spill more hydrogen species over the support to reduce Ce<sup>4+</sup>. This result is well consistent with that in literature [48], which indicates that the supported Au could promote the reduction of Ce<sup>4+</sup>. Moreover, it is also pointed out that the reduction of the reducible supports (e.g., Ce<sup>4+</sup>) could contribute to inhibit sintering of Au particle in the process of catalyst activation. This can further explain the better dispersion of Au on Ce<sub>0.4</sub>Zr<sub>0.6</sub>O<sub>2</sub> support. The O<sub>1s</sub> peaks of Au/Ce<sub>x</sub>Zr<sub>1-x</sub>O<sub>2</sub> catalyst are shown in Figure 5b. Two oxygen species can be found, and

the peak with low binding energy at 527.4 eV is attributed to the oxygen ions in the crystal lattice ( $O_I$ ), and the high binding energy at around 530 eV is assigned to the adsorbed oxygen species ( $O_{II}$ ). In the case of  $Ce_{0.4}Zr_{0.6}O_2$  support, the highest  $O_{II}$  percentage is obtained (Table S3). However, the greatest decrease of  $O_{II}$  percentage is observed over  $Au/Ce_{0.4}Zr_{0.6}O_2$  catalyst after reduction, probably owing to the easy reduction of Au resulting in the further reduction of adsorbed oxygen in the presence of excessive  $H_2$ .

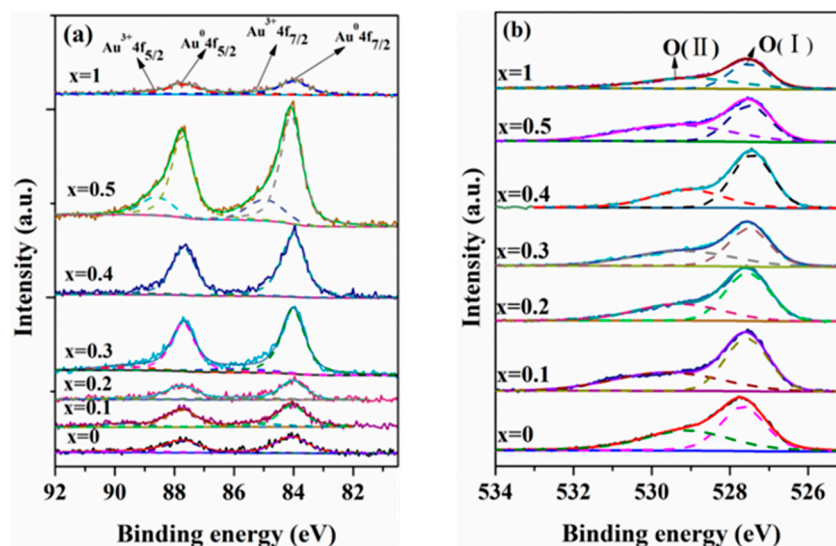


Figure 5. XP spectra of the (a) Au(4f) and (b) O(1s) of 0.6 wt % Au supported on  $Ce_xZr_{1-x}O_2$ .

## 2.2. GVL Production from LA and FA

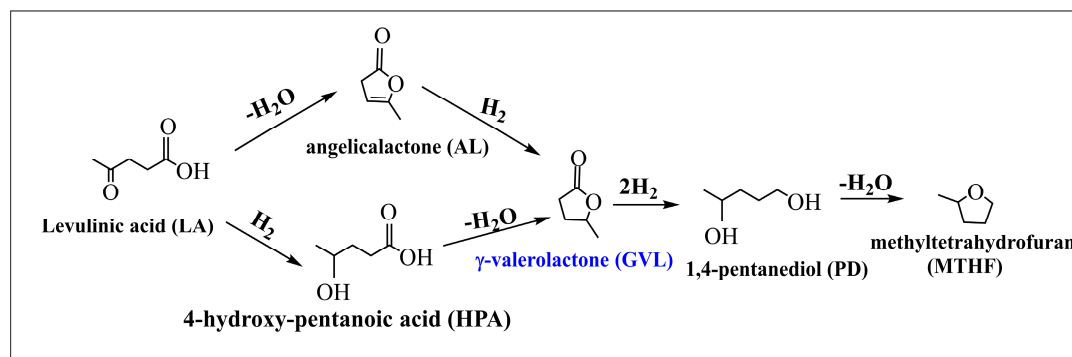
### 2.2.1. FA Decomposition

Formic acid is a potential hydrogen source, owing to the environmentally friendly property and easy production from biomass treatment. The decomposition of formic acid can pass through a pathway of dehydrogenation reaction ( $HCOOH(l) \rightarrow H_2(g) + CO_2(g)$ ,  $\Delta G_{298K} = -35.0 \text{ kJ}\cdot\text{mol}^{-1}$ ) or a dehydration pathway ( $HCOOH(l) \rightarrow H_2O(l) + CO(g)$ ,  $\Delta G_{298K} = -14.9 \text{ kJ}\cdot\text{mol}^{-1}$ ) [49], depending on the employed catalyst and reaction conditions. The decomposition of FA is very slow in the absence of the catalyst, which slightly increases from 2.2% at 120 °C to 34.7% at 240 °C. In addition, no CO is detected at 120 °C. However, CO can be produced at temperatures higher than 150 °C. With the addition of  $Au/CeO_2$ , the conversion of FA exhibits a slight increase.  $Au/ZrO_2$  shows much better levels of efficiency than  $Au/CeO_2$  for FA decomposition. When  $Au/Ce_xZr_{1-x}O_2$  catalyst is adopted, the highest conversion of FA is obtained. The conversion of FA significantly increases with increasing Ce content, and gets the maximum of 87% over  $Au/Ce_{0.4}Zr_{0.6}O_2$ , then sharply decreases to only 24.8% in the presence of pure  $CeO_2$  at 160 °C. The best activity of  $Au/Ce_{0.4}Zr_{0.6}O_2$  for FA decomposition is possibly attributed to the well-dispersed Au on  $Ce_{0.4}Zr_{0.6}O_2$  support. Iglesia et al. also shows the higher activity of well-dispersed Au species than Pt cluster to decompose FA [50]. Moreover, the selectivity to  $H_2$  shows obvious increase, and no CO is detected. This suggests that doping a certain amount of Ce into  $ZrO_2$  favors both FA conversion and  $H_2$  production. When the reaction temperature is beyond 210 °C, FA can be completely decomposed over  $Au/Ce_{0.4}Zr_{0.6}O_2$  without CO formation.

### 2.2.2. GVL Production

Based on the good performance of  $Au/Ce_xZr_{1-x}O_2$  on FA decomposition to yield  $H_2$ , the production of GVL directly from biomass-based LA and FA are investigated over the  $Au/Ce_xZr_{1-x}O_2$  catalyst. The effect of Ce content on GVL formation is shown in Table 2. When 0.6 wt %  $Au/ZrO_2$  is used as the catalyst, 40.7% of LA is converted, and the yield and selectivity of GVL are 36.4% and

89.5%, respectively. With the introduction of Ce into the supports, the conversion of LA gradually increases and gets the maximum (63.5%) over the 0.6 wt % Au/Ce<sub>0.4</sub>Zr<sub>0.6</sub>O<sub>2</sub> catalyst, and GVL yield is raised to 49.7%. However, more doped Ce leads to the significant decrease of both LA conversion and GVL yield. For example, only 13.1% of LA is converted and 9.2% of GVL is obtained over the 0.6 wt % Au/CeO<sub>2</sub> catalyst, although all of the FA is decomposed to H<sub>2</sub> under the similar conditions. This indicates that the support greatly influences the conversion of LA to produce GVL. There are two possible pathways for LA conversion to GVL in literature [51]. One pathway involves the hydrogenation of LA to 4-hydroxy-pentanoic acid (HPA), and then HPA is further converted to GVL via the intra-molecular lactonization reaction. The other involves the formation of intermediate angelica lactone by dehydration of LA with acid catalysis, and then angelica lactone is further hydrogenated to form GVL. For both of these pathways, the active metal and acidic sites is required on the catalyst surface. The active metal can catalyze the hydrogenation of LA or the intermediate angelica lactone, which is commonly recognized as the rate-determining step, whereas the acidic sites mainly contribute to the dehydration reaction. It is known that the polymerization of angelica lactone promoted by the acidic catalysis leads to the formation of coke, while the pathway passing through angelica lactone is usually considered as the predominant way [52]. Furthermore, the intermediates including both angelica lactone and 4-hydroxy-pentanoic acid are indeed detected when the Au/Ce<sub>0.4</sub>Zr<sub>0.6</sub>O<sub>2</sub> catalyst is used in our work, indicating that the formation of GVL might pass through both the pathways (Scheme 1). In addition to GVL, several by-products such as methyl-tetrahydrofuran (MTHF), 1,4-pentanediol (PD) were detected by HPLC. However, the amounts of by-products with small molecular weight are very limited. An obvious peak that cannot be identified was also found by HPLC analysis. However, further analysis by GC-MS indicates that no other obvious peaks are found except for MTHF, PD and limited intermediates. It is therefore speculated that the main by-products possibly include some polymer and /or coke that is difficult to be quantified.



**Scheme 1.** The possible reaction pathway of GVL production from LA and FA.

**Table 2.** The effect of doped Ce on the conversion of LA to GVL at 240 °C for 2 h<sup>a</sup>.

Catalyst <sup>b</sup>	C <sub>FA</sub> (%) <sup>c</sup>	C <sub>LA</sub> (%) <sup>d</sup>	Y <sub>GVL</sub> (%) <sup>e</sup>	S <sub>GVL</sub> (%) <sup>f</sup>	C <sub>PD</sub> <sup>g</sup>
Au/ZrO <sub>2</sub>	99.9	40.7	36.4	89.5	trace
Au/Ce <sub>0.1</sub> Zr <sub>0.9</sub> O <sub>2</sub>	100	47.0	33.6	82.6	trace
Au/Ce <sub>0.2</sub> Zr <sub>0.8</sub> O <sub>2</sub>	100	51.7	43.1	83.4	trace
Au/Ce <sub>0.3</sub> Zr <sub>0.7</sub> O <sub>2</sub>	100	60.3	46.8	77.6	trace
Au/Ce <sub>0.4</sub> Zr <sub>0.6</sub> O <sub>2</sub>	100	63.5	49.7	77.3	trace
Au/Ce <sub>0.5</sub> Zr <sub>0.5</sub> O <sub>2</sub>	100	55.4	37.1	67.0	trace
Au/CeO <sub>2</sub>	95.6	13.1	9.2	70.2	trace

<sup>a</sup> Reaction conditions: 22.4 mmol LA, 22.4 mmol FA, 50 mL H<sub>2</sub>O, 0.25 g catalyst, 240 °C and 2 h; <sup>b</sup> Au loading was 0.6 wt %; <sup>c</sup> Conversion of FA; <sup>d</sup> Conversion of LA; <sup>e</sup> The yield of GVL; <sup>f</sup> The selectivity of GVL; <sup>g</sup> The concentration of 1,4-pentanediol.

Combined with the results of catalyst characterization, we can find that the addition of a certain amount of Ce could facilitate the formation of tetragonal phase support, which is recognized as the most desired structures on LA conversion to GVL [53]. Therefore, higher GVL yields are obtained over Au/Ce<sub>0.4</sub>Zr<sub>0.6</sub>O<sub>2</sub>. However, the pure tetragonal phase is easily transformed into the monoclinic and cubic phase. In the case of the pure ZrO<sub>2</sub> or Ce<sub>x</sub>Zr<sub>1-x</sub>O<sub>2</sub> solid solution with  $x > 0.5$ , monoclinic or cubic phases are obtained respectively, thereby reducing the catalytic activity and GVL yield. In addition, the doped Ce can promote the reduction of Au<sup>n+</sup> to metallic Au<sup>0</sup>, and also benefits the dispersion of Au, yielding small Au nanoparticles with the mean size of about 2.4 nm. Consequently, more metal Au<sup>0</sup> are obtained and contribute to the higher decomposition of FA to H<sub>2</sub>, as well as the better hydrogenation ability of LA to form GVL. Moreover, the lowest percentage of O<sub>II</sub> is observed over Au/Ce<sub>0.4</sub>Zr<sub>0.6</sub>O<sub>2</sub> catalyst. It is reported that the adsorbed oxygen is corresponding to the oxygen species trapped by oxygen vacancies [54,55]. For the sample of Au/Ce<sub>x</sub>Zr<sub>1-x</sub>O<sub>2</sub> catalyst, oxygen vacancies are originated from the reduction of Ce<sup>4+</sup> to Ce<sup>3+</sup> [56]. It is reported that the oxygen vacancy could stabilize the -C=O in LA via the strong interaction with oxygen deficient, thereby decreasing the reaction activity for hydrogenation [57]. Thus, the lowest percentage of O<sub>II</sub> in Au/Ce<sub>0.4</sub>Zr<sub>0.6</sub>O<sub>2</sub> catalyst can render the least inactivation of -C=O in LA, favoring the further hydrogenation reaction. The acidity of the Ce<sub>0.4</sub>Zr<sub>0.6</sub>O<sub>2</sub> solid solution, especially the moderate and weak acids, is the highest among the adopted supports. According to the proposed reaction pathway (Scheme 1), it can be known that higher acid amount can significantly promote the molecular dehydration reaction of LA hydrogenation products, thereby further improving the yield of GVL. This is well in line with the result in literature that medium-strength acid is important for LA conversion to GVL [12,28]. Weckhuysen et al. points out that the presence of a strong acid could lead to the hydrogenation of LA, passing through the formation of 4-hydroxypentanoic acid (HPA) and pentanoic acid [34]. However, no pentanoic acid is obtained in this work, verifying the limited strong acid in the prepared catalyst (Figure 3). Therefore, it is believed that Au/Ce<sub>0.4</sub>Zr<sub>0.6</sub>O<sub>2</sub> is a multifunctional catalyst, where the metal sites and acidic sites exhibit synergistic effects for GVL production from LA and FA. The performance of Au/Ce<sub>0.4</sub>Zr<sub>0.6</sub>O<sub>2</sub> includes the promotion of FA decomposition to produce H<sub>2</sub> and the reduction of carbonyl group. The oxygen of the ketone groups could be combined to the acid sites of Ce<sub>0.4</sub>Zr<sub>0.6</sub>O<sub>2</sub> support, thus weakening -C=O bond. This could make -C=O more susceptible to hydrogenation, therefore facilitating the next dehydration reaction to form GVL.

The performance of Au/Ce<sub>0.4</sub>Zr<sub>0.6</sub>O<sub>2</sub> catalyst on the conversion of LA to GVL with FA as hydrogen source is greatly relied on the Au loading (Figure 6). An increase of actual Au loading to 2.0 wt % contributes to the increase of GVL yield. The highest yield of GVL (83.5%) with 92% selectivity is achieved over 2 wt % Au/Ce<sub>0.4</sub>Zr<sub>0.6</sub>O<sub>2</sub> catalyst. Based on the calculated gold atoms on the surface of catalyst via the hemispherical ball model [58], the total turnover number (TON), which implies the ratio of molar amount of GVL formed to that of active Au site, is estimated to be 2047.8, whereas the TON value is only 1468 in the case of Au/ZrO<sub>2</sub>. When the Au loading is increased to 2.2 wt %, both LA conversion and GVL yield show a slight decrease, owing to the aggregation of Au on the supports (Figure 1B). Additionally, reaction temperature and time can also influence the GVL production. Both LA conversion and GVL yield gradually increase with the increasing reaction temperature, and a satisfied yield of GVL (83.5%) is obtained at 240 °C. However, the further increase of reaction temperature to 280 °C leads to the sharp decrease of GVL yield and selectivity. This can be ascribed to two possible reasons. One relates to the fact that higher temperature is not conducive to the hydrogenation of LA. The other involves the further decomposition of GVL at higher temperature, where the by-product 1,4-pentanediol derived from deep hydrogenation is observed. Therefore, 240 °C is considered to be the optimum reaction temperature. At 240 °C the conversion of LA reaches the maximum (90.8%) after 2 h. However, longer reaction time results in the slight increase of LA conversion but much lower GVL yield and selectivity. This decrease may be attributed to the further hydrogenation of GVL to MTHF.

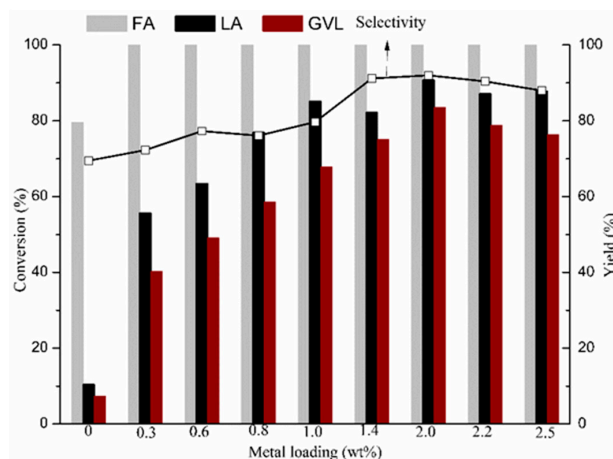


**Figure 6.** The effect of Au loading on the conversion of LA to GVL at 240 °C for 2 h.

### 2.3. Recyclability of the Catalyst

The recyclability of Au/Ce<sub>0.4</sub>Zr<sub>0.6</sub>O<sub>2</sub> catalyst is investigated (Figure 7). In each cycle, we recovered the catalyst by centrifugation. The recovered catalyst is then sequentially washed with pure water and ethanol. After drying at room temperature, the catalyst is directly reused for the next run without further reduction. In the second run, there is a slight decrease for LA conversion and GVL yield. However, in the following runs, no obvious loss of the catalytic activity is observed, indicating the good stability of the catalyst. The Au concentration in liquid phase is below the detection limits of ICP analysis. This might be ascribed to the fact that the doped Ce can stabilize the Au/Ce<sub>0.4</sub>Zr<sub>0.6</sub>O<sub>2</sub> catalyst by enhancing the interaction of support-metal [54], thereby reducing the leaching of metal Au in the process of GVL production in acidic aqueous solution. The relative concentration of metallic Au<sup>0</sup> (89.0%) after five runs shows no obvious change compared to the fresh catalyst (89.4%) (Figure S3). In addition, the TEM analysis (Figure 4d) of Au/Ce<sub>0.4</sub>Zr<sub>0.6</sub>O<sub>2</sub> catalyst after five runs displays a mean Au particle size concentrating around 2.6 nm and is well distributed. The XRD of the spent catalysts after five cycles is also conducted. As shown in Figure 1B-i, the characteristic diffraction peak of Au shows no obvious change, and only a slight decrease of the tetragonal phase of support on the surface of catalyst is observed. Zhang et al. indicates that the formation of tetragonal phase can increase the stability, attributing to the strong metal–support interaction [15]. Therefore, it can be considered that the limited decrease of catalytic activity is possibly ascribed to the slight increase in Au<sup>0</sup> particle size and the decrease of tetragonal phase of the support.

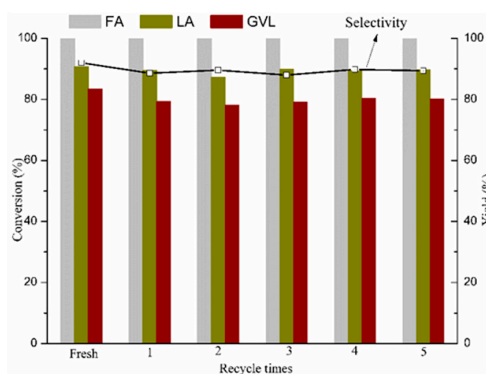


**Figure 7.** The recyclability of catalyst (Reaction conditions: 22.4 mmol LA, 22.4 mmol FA, 50 mL H<sub>2</sub>O, 0.25 g catalyst, 240 °C and 2 h).

### 3. Methods Experimental Section

#### 3.1. Materials

Noble metal precursor  $\text{HAuCl}_4 \cdot 4\text{H}_2\text{O}$  was purchased from Xiya Regent Co (99.5%, Shandong, China). Formic acid (FA, 97%),  $\text{Ce}(\text{NO}_3)_3 \cdot 6\text{H}_2\text{O}$  and  $\text{Zr}(\text{NO}_3)_4 \cdot 5\text{H}_2\text{O}$  were purchased from Kelong Chemical Regent Factory (Chengdu, China). Levulinic acid (LA, 99%) was obtained from J&K Scientific Ltd. (Beijing, China).

#### 3.2. Methods

##### 3.2.1. Catalyst Preparation

$\text{ZrO}_2$  support:  $\text{ZrO}_2$  powder was prepared via a precipitation method in literature [23]. Typically, 12.9 g  $\text{ZrOCl}_2 \cdot 8\text{H}_2\text{O}$  was dissolved in 200 mL deionized water at ambient temperature. Then, we adjusted the pH of solution to 9.0 by adding 2.5 M  $\text{NH}_3 \cdot \text{H}_2\text{O}$ . The resulted hydrogel was then washed with deionized water. The obtained precipitate was dried at 110 °C overnight, and then calcined in a tube furnace at 400 °C for 2 h in air.

$\text{Ce}_x\text{Zr}_{1-x}\text{O}_2$  support: The solid solutions  $\text{Ce}_x\text{Zr}_{1-x}\text{O}_2$  ( $x_{\text{molar}}$  ratio of Ce/Zr = 0.1, 0.2, 0.3, 0.4, 0.5) were prepared via a coprecipitation method. The starting metal salts ( $\text{Zr}(\text{NO}_3)_4 \cdot 5\text{H}_2\text{O}$ ,  $\text{Ce}(\text{NO}_3)_3 \cdot 6\text{H}_2\text{O}$ ) were firstly dissolved in distilled water to the desired concentration, and then the pH of mixture was altered to 9.0 with 2.5 M ammonia. The mixture was kept at 70 °C for 2 h. Then, the mixture was cooled to ambient temperature and set for 12 h. The mixture was centrifuged. The resulted gel was washed with deionized water, and then dried overnight at 110 °C, and then calcined at 450 °C for 4 h in a tube furnace. The preparation method of  $\text{CeO}_2$  support is similar to that of  $\text{ZrO}_2$ .

$\text{Au}/\text{Ce}_x\text{Zr}_{1-x}\text{O}_2$  and  $\text{Au}/\text{ZrO}_2$  catalysts: the catalyst was prepared using deposition-precipitation (DP) method. Firstly, the support was mixed with appropriate amounts of chloroauric acid aqueous solution (1 mM). The pH of the solution was adjusted to 9.0 with 0.25 M ammonia. Then, the mixture was stirred at ambient temperature for 6 h. The obtained sample was washed with deionized water for five times, and then was separated by filtration. After drying at 80 °C in oven for 1 h, the obtained catalyst was pre-reduced before reaction using 5%  $\text{H}_2/\text{Ar}$  at 350 °C for 2 h.

##### 3.2.2. Catalyst Characterization

We used the  $\text{N}_2$  adsorption-desorption to determine the BET specific surface areas of samples at 77 K by a Micromeritics Tristar II 3020 analyzer (Micromeritics, Atlanta, GA, USA). Before analysis, 0.15 g samples were heated to 393 K and kept for 2 h. Then, the samples were further heated to 573 K for 2 h to remove the physically adsorbed impurities in vacuum. The specific surface areas and pore volumes were calculated by the BET equation and BJH method, respectively [36].

The samples were conducted by X-ray diffraction (XRD) measurements on a Dandong Fangyuan DX-1000 instrument. The monochromatic Cu  $K\alpha$  radiation with  $\lambda = 1.542 \text{ \AA}$  (40 kV and 25 mA) was employed, and the scanning range of  $2\theta$  was ranging from 10° to 80°.

The composition in the bulk of catalyst was determined by X-ray fluorescent spectroscopy (XRF) using Shimadzu XRF-1800 (40 kV and 95 mA), Japan.

We used Raman spectra to characterize the catalysts on a HOLIBA R-XploRA instrument equipped with an optical microscope (BX41, Olympus). The excitation wavelength was set at 532 nm. For each spectrum, an average of 5 scans was obtained with grating of 1800 gr/mm in the 150–1000  $\text{cm}^{-1}$  range.

Transmission electron microscopy (TEM) was used to examine the surface morphology and the mean particle size of the samples, using an Tecnai G2F20 instrument (FEI, Hillsboro, OR, USA). Before TEM analysis, the catalysts were ultrasonically dispersed in ethanol solvent for 1 h at room temperature, and then the resulted solution was deposited onto copper grids.

XPS analysis was carried out using an Axis Ultra DLD spectrometer (Kratos, UK) equipped with an Al-K $\alpha$  X-ray radiation. The C1s peak was set at 284.6 eV, and then the energy scale was internally calibrated.

Inductively coupled plasma atomic emission spectroscopy (ICP-AES) with a Thermo Elemental IRIS Advantage ER/S spectrometer (Spectro, Kleve, Germany) was used to determine the actual Au loading of the catalyst. Before analysis, 0.1 g catalyst was dissolved in aqua regia and diluted to 100 mL with water, and then the leaching of Au in the filtrate liquid was determined.

NH<sub>3</sub>-temperature-programmed desorption (NH<sub>3</sub>-TPD) was conducted to determine the acidic properties of the samples, using Micromeritics Autochem II 2920 instrument (Micromeritics Instrument Corp., Norcross, GA, USA). Before analysis, 100 mg samples were pretreated in the helium flow with a rate of 30 mL·min<sup>-1</sup> at 500 °C for 4 h, and then was cooled to 100 °C. Ammonia adsorption was carried out in 10% NH<sub>3</sub>-helium (25 mL·min<sup>-1</sup>) at 100 °C for 4 h. Subsequently, we removed the excessive physisorbed ammonia by helium at 100 °C for 2 h, and the helium flow rate was 30 mL·min<sup>-1</sup>. Then, the temperature was raised from 100 to 600 °C (10 °C·min<sup>-1</sup>).

H<sub>2</sub>-temperature-programmed reduction (H<sub>2</sub>-TPR) of the catalyst was conducted using a Micromeritics Autochem II 2920 instrument. The catalyst (100 mg) was firstly pretreated in a flow of argon at 150 °C for 1 h, and then cooling to 35 °C. Subsequently, the tests were carried out by increasing the temperature from 35 to 800 °C with a rate of 8 °C·min<sup>-1</sup> in a flow of 10% H<sub>2</sub>-Ar (50 mL·min<sup>-1</sup>).

### 3.2.3. Conversion of LA to GVL

The production of GVL from LA was carried at a high-pressure Parr reactor with stirring at a rate of 400 rpm. FA was employed as the hydrogen source, and Au/Ce<sub>x</sub>Zr<sub>1-x</sub>O<sub>2</sub> (x = 0, 0.1, 0.2, 0.3, 0.4, 0.5, 1) was used as the catalyst. In a typical run, 50 mL water, LA (22.4 mmol), FA (22.4 mmol) and 0.25 g catalyst were mixed in reactor. The air in reactor was replaced by nitrogen for three minutes with the initial pressure of 1.0 MPa. Then the reaction temperature was raised to the designed temperature, and kept until the reaction was complete. After that, we cooled the reactor to ambient temperature. The obtained gases were analyzed by GC with TCD. The mixture in the reactor was poured out, and then deionized water was employed to wash the reactor for three times. After filtration, the solid catalyst was separated from the liquid mixture. Ethanol was used to wash the separated catalyst. The catalyst can be reused after drying at 80 °C. The obtained products were determined by HPLC. Formic acid, levulinic acid and  $\gamma$ -valerolactone were detected by UV detector at the wavelength of 210 nm, and all samples were determined by standard curve method. The yield and selectivity of GVL are defined as the following:

$$\text{Yield (mol\%)} = \frac{\text{GVL amount (mol)}}{\text{The amount of LA used (mol)}} \times 100\% \quad (1)$$

$$\text{selectivity (mol\%)} = \frac{\text{GVL amount (mol)}}{\text{The amount of converted LA (mol)}} \times 100\% \quad (2)$$

## 4. Conclusions

It is found that the Ce/Zr ratio greatly influences the morphology and activity of Au/Ce<sub>x</sub>Zr<sub>1-x</sub>O<sub>2</sub> catalysts for the production of GVL from biomass-based LA and equivalent molar FA without extra hydrogen source. The catalyst with an optimal Ce/Zr molar ratio of 4:6 (Au/Ce<sub>0.4</sub>Zr<sub>0.6</sub>O<sub>2</sub>) exhibits the highest catalytic activity, and 90.8% of LA conversion and 83.5% of GVL yield could be achieved under the optimum reaction conditions. The doped Ce could facilitate the formation of tetragonal phase of support, and increase the amounts of weak and medium-strength acidic sites. In addition, the doped Ce can promote the reduction of Au<sup>n+</sup> to metallic Au<sup>0</sup>, and promote the dispersion of Au<sup>0</sup>. The formation of tetragonal phase, higher acidity, and high Au<sup>0</sup> percentage are considered to contribute to the high efficiency of Au/Ce<sub>0.4</sub>Zr<sub>0.6</sub>O<sub>2</sub> for GVL production. There is no notable decrease for catalytic activity of catalyst after 5 runs, indicating good stability.

**Supplementary Materials:** The following are available online at <http://www.mdpi.com/2073-4344/8/6/241/s1>, Figure S1: Pore size distribution and N<sub>2</sub> adsorption-desorption isotherms for samples of 0.6 wt % Au catalyst supported on Ce<sub>x</sub>Zr<sub>1-x</sub>O<sub>2</sub>, Figure S2: XP spectra of the Ce (3d) of (a) Ce<sub>x</sub>Zr<sub>1-x</sub>O<sub>2</sub> and (b) 0.6 wt % Au/Ce<sub>x</sub>Zr<sub>1-x</sub>O<sub>2</sub>, Figure S3: XP spectra of 2 wt % Au/Ce<sub>0.4</sub>Zr<sub>0.6</sub>O<sub>2</sub> catalyst: (a) before reaction; (b) after five runs, Table S1: BET analysis and H<sub>2</sub> consumption from TPR of 0.6 wt % Au/Ce<sub>x</sub>Zr<sub>1-x</sub>O<sub>2</sub>, Table S2: The relative concentration of surface cerium species on different supports and catalysts, Table S3: The relative concentration of surface O1s on different supports and catalysts.

**Author Contributions:** C.H. and J.L. designed the experiments; X.L. (Xiaoling Li), X.L. (Xudong Liu), Q.T. conducted the experiments; X.L. (Xiaoling Li), J.L. and C.H. analyzed the data and co-wrote the paper.

**Acknowledgments:** This work is financially supported by the National Natural Science Foundation of China (No. 21606155), the 111 project (B17030), Application Foundation Program of Sichuan Province (No. 2016)Y0189), and the Basic scientific research fund of MOE. The characterization from the Analytical and Testing Center of Sichuan University is greatly appreciated.

**Conflicts of Interest:** There are no conflicts to declare.

## References

1. Du, X.-L.; He, L.; Zhao, S.; Liu, Y.-M.; Cao, Y.; He, H.-Y.; Fan, K.-N. Hydrogen-Independent reductive transformation of carbohydrate biomass into  $\gamma$ -valerolactone and pyrrolidone derivatives with supported gold catalysts. *Angew. Chem.* **2011**, *123*, 7961–7965. [[CrossRef](#)]
2. Alonso, D.M.; Wettstein, S.G.; Dumesic, J.A. Gamma-valerolactone, a sustainable platform molecule derived from lignocellulosic biomass. *Green Chem.* **2013**, *15*, 584–595. [[CrossRef](#)]
3. Wettstein, S.G.; Alonso, D.M.; Gürbüz, E.I.; Dumesic, J.A. A roadmap for conversion of lignocellulosic biomass to chemicals and fuels. *Curr. Opin. Chem. Eng.* **2012**, *1*, 218–224. [[CrossRef](#)]
4. Wright, W.R.H.; Palkovits, R. Development of heterogeneous catalysts for the conversion of levulinic acid to  $\gamma$ -valerolactone. *ChemSusChem* **2012**, *5*, 1657–1667. [[CrossRef](#)] [[PubMed](#)]
5. Zhang, J.; Wu, S.; Li, B.; Zhang, H. Advances in the catalytic production of valuable levulinic acid derivatives. *ChemCatChem* **2012**, *4*, 1230–1237. [[CrossRef](#)]
6. Yan, K.; Yang, Y.; Chai, J.; Lu, Y. Catalytic reactions of gamma-valerolactone: A platform to fuels and value-added chemicals. *Appl. Catal. B* **2015**, *179*, 292–304. [[CrossRef](#)]
7. Luo, W.; Sankar, M.; Beale, A.M.; He, Q.; Kiely, C.J.; Buijneninx, P.C.A.; Weckhuysen, B.M. High performing and stable supported nano-alloys for the catalytic hydrogenation of levulinic acid to  $\gamma$ -valerolactone. *Nat. Commun.* **2015**, *6*, 6540–6550. [[CrossRef](#)] [[PubMed](#)]
8. Wang, A.; Lu, Y.; Yi, Z.; Ejaz, A.; Hu, K.; Zhang, L.; Yan, K. Selective Production of  $\gamma$ -Valerolactone and Valeric Acid in One-Pot Bifunctional Metal Catalysts. *ChemistrySelect* **2018**, *3*, 1097–1101. [[CrossRef](#)]
9. Yan, K.; Liu, Y.; Lu, Y.; Chaib, J.; Suna, L. Catalytic application of layered double hydroxide-derived catalysts for the conversion of biomass derived molecules. *Catal. Sci. Technol.* **2017**, *7*, 1622–1645. [[CrossRef](#)]
10. Osatiashtiani, A.; Flee, A.; Wilson, K. Recent advances in the production of  $\gamma$ -valerolactone from biomass-derived feedstocks via heterogeneous catalytic transfer hydrogenation. *J. Chem. Technol. Biotechnol.* **2017**, *92*, 1125–1135. [[CrossRef](#)]
11. Chia, M.; Dumesic, J.A. Liquid-phase catalytic transfer hydrogenation and cyclization of levulinic acid and its esters to  $\gamma$ -valerolactone over metal oxide catalysts. *Chem. Commun.* **2011**, *47*, 12233–12235. [[CrossRef](#)] [[PubMed](#)]
12. Zhu, S.; Xue, Y.; Guo, J.; Cen, Y.; Wang, J.; Fan, W. Integrated Conversion of Hemicellulose and Furfural into  $\gamma$ -Valerolactone over Au/ZrO<sub>2</sub> Catalyst Combined with ZSM-5. *ACS Catal.* **2016**, *6*, 2035–2042. [[CrossRef](#)]
13. Liguori, F.; Moreno-Marrodan, C.; Barbaro, P. Environmentally Friendly Synthesis of  $\gamma$ -Valerolactone by Direct Catalytic Conversion of Renewable Sources. *ACS Catal.* **2015**, *5*, 1882–1894. [[CrossRef](#)]
14. Fábos, V.; Mika, L.T.; Horváth, I.T. Selective Conversion of Levulinic and Formic Acids to  $\gamma$ -Valerolactone with the Shvo Catalyst. *Organometallics* **2014**, *33*, 181–187. [[CrossRef](#)]
15. Deuss, P.J.; Barta, K.; de Vries, J.G. Homogeneous catalysis for the conversion of biomass and biomass-derived platform chemicals. *Catal. Sci. Technol.* **2014**, *4*, 1174–1196. [[CrossRef](#)]
16. Horváth, I.T.; Mehdi, H.; Fabos, V.; Boda, L.; Mika, L.T.  $\gamma$ -Valerolactone—A sustainable liquid for energy and carbon-based chemicals. *Green Chem.* **2008**, *10*, 238–242. [[CrossRef](#)]

17. Deng, L.; Zhao, Y.; Li, J.; Fu, Y.; Liao, B.; Guo, Q.X. Conversion of Levulinic Acid and Formic Acid into  $\gamma$ -Valerolactone over Heterogeneous Catalysts. *ChemSusChem* **2010**, *3*, 1172–1175. [[CrossRef](#)] [[PubMed](#)]
18. Cao, W.; Luo, W.; Ge, H.; Su, Y.; Wang, A.; Zhang, T. UiO-66 derived Ru/ZrO<sub>2</sub>@C as a highly stable catalyst for hydrogenation of levulinic acid to  $\gamma$ -valerolactone. *Green Chem.* **2017**, *19*, 2201–2211. [[CrossRef](#)]
19. Alonso, D.M.; Wettstein, S.G.; Bond, J.Q.; Root, T.W.; Dumesic, J.A. Production of Biofuels from Cellulose and Corn Stover Using Alkylphenol Solvents. *ChemSusChem* **2011**, *4*, 1078–1081. [[CrossRef](#)] [[PubMed](#)]
20. Braden, D.J.; Henao, C.A.; Heltzel, J.; Maravelias, C.C.; Dumesic, J.A. Production of liquid hydrocarbon fuels by catalytic conversion of biomass-derived levulinic acid. *Green Chem.* **2011**, *13*, 1755–1765. [[CrossRef](#)]
21. Sen, S.M.; Henao, C.A.; Braden, D.J.; Dumesic, J.A.; Maravelias, C.T. Catalytic conversion of lignocellulosic biomass to fuels: Process development and techno-economic evaluation. *Chem. Eng. Sci.* **2012**, *67*, 57–67.
22. Serrano-Ruiz, J.C.; Wang, D.; Dumesic, J.A. Catalytic upgrading of levulinic acid to 5-nonanone. *Green Chem.* **2010**, *12*, 574–577. [[CrossRef](#)]
23. Yan, Z.P.; Lin, L.; Liu, S. Synthesis of  $\gamma$ -Valerolactone by Hydrogenation of Biomass-derived Levulinic Acid over Ru/C Catalyst. *Energy Fuels* **2009**, *23*, 3853–3858. [[CrossRef](#)]
24. Zacharska, M.; Chuvilin, A.L.; Kriventsov, V.V.; Beloshapkin, S.; Estrada, M.; Simakov, A.; Bulushev, D.A. Support effect for nanosized Au catalysts in hydrogen production from formic acid decomposition. *Catal. Sci. Technol.* **2016**, *6*, 6853–6860. [[CrossRef](#)]
25. Yuan, J.; Li, S.; Yu, L.; Liu, Y.; Cao, Y.; He, H.; Fan, K. Copper-based catalysts for the efficient conversion of carbohydrate biomass into  $\gamma$ -valerolactone in the absence of externally added hydrogen. *Energy Environ. Sci.* **2013**, *6*, 3308–3313. [[CrossRef](#)]
26. Kumar, V.V.; Naresh, G.; Sudhakar, M.; Anjaneyulu, C.; Bhargava, S.K.; Tardio, J.; Reddy, V.K.; Padmasri, A.H.; Venugopal, A. An investigation on the influence of support type for Ni catalysed vapour phase hydrogenation of aqueous levulinic acid to  $\gamma$ -valerolactone. *RSC Adv.* **2016**, *6*, 9872–9879. [[CrossRef](#)]
27. Lomate, S.; Sultana, A.; Fujitani, T. Effect of SiO<sub>2</sub> support properties on the performance of Cu–SiO<sub>2</sub> catalysts for the hydrogenation of levulinic acid to gamma valerolactone using formic acid as a hydrogen source. *Catal. Sci. Technol.* **2017**, *7*, 3073–3083. [[CrossRef](#)]
28. Ruppert, A.M.; Grams, J.; Jędrzejczyk, M.; Matras-Michalska, J.; Keller, N.; Ostojka, K.; Sautet, P. Titania-Supported Catalysts for Levulinic Acid Hydrogenation: Influence of Support and its Impact on  $\gamma$ -Valerolactone Yield. *ChemSusChem* **2015**, *8*, 1538–1547. [[CrossRef](#)] [[PubMed](#)]
29. Valekar, A.H.; Cho, K.; Chitale, S.K.; Hong, D.; Cha, G.; Lee, U.; Hwang, D.W.; Serre, C.; Chang, J.; Hwang, Y.K. Catalytic transfer hydrogenation of ethyl levulinate to  $\gamma$ -valerolactone over zirconium-based metal–organic frameworks. *Green Chem.* **2016**, *18*, 4542–4552. [[CrossRef](#)]
30. Lange, J.P.; Price, R.; Ayoub, P.; Louis, J.; Petrus, L.; Clarke, L.; Gosselink, H. Valeric Biofuels: A Platform of Cellulosic Transportation Fuels. *Angew. Chem. Int. Ed.* **2010**, *49*, 4479–4483. [[CrossRef](#)] [[PubMed](#)]
31. Luo, W.; Deka, U.; Beale, A.M.; Eck, E.R.H.V.; Bruijninx, P.C.A.; Weckhuysen, B.M. Ruthenium-catalyzed hydrogenation of levulinic acid: Influence of the support and solvent on catalyst selectivity and stability. *J. Catal.* **2013**, *301*, 175–186. [[CrossRef](#)]
32. Abdelrahman, O.A.; Luo, H.Y.; Heyden, A.; Román-Leshkov, Y.; Bond, J.Q. Toward rational design of stable supported metal catalysts for aqueous-phase processing: Insights from the hydrogenation of levulinic acid. *J. Catal.* **2015**, *329*, 10–21. [[CrossRef](#)]
33. Ftouni, J.; Muñoz-Murillo, A.; Goryachev, A.; Hofmann, J.P.; Hensen, E.J.M.; Lu, L.; Kiely, C.J.; Bruijninx, P.C.A.; Weckhuysen, B.M. ZrO<sub>2</sub> is Preferred over TiO<sub>2</sub> as Support for the Ru-Catalyzed Hydrogenation of Levulinic Acid to  $\gamma$ -Valerolactone. *ACS Catal.* **2016**, *6*, 5462–5472. [[CrossRef](#)]
34. Deng, L.; Li, J.; Lai, D.M.; Fu, Y.; Guo, Q.X. Catalytic Conversion of Biomass-Derived Carbohydrates into  $\gamma$ -Valerolactone without Using an External H<sub>2</sub> Supply. *Angew. Chem.* **2009**, *121*, 6651–6654. [[CrossRef](#)]
35. Luo, W.; Bruijninx, P.C.A.; Weckhuysen, B.M. Selective, one-pot catalytic conversion of levulinic acid to pentanoic acid over Ru/H-ZSM5. *J. Catal.* **2014**, *320*, 33–41. [[CrossRef](#)]
36. Luo, Y.; Yi, J.; Tong, D.; Hu, C. Production of  $\gamma$ -valerolactone via selective catalytic conversion of hemicellulose in pubescens without addition of external hydrogen. *Green Chem.* **2016**, *18*, 848–857. [[CrossRef](#)]
37. Pengpanich, S.; Meeyoo, V.; Rirksomboon, T.; Bunyakiat, K. Catalytic oxidation of methane over CeO<sub>2</sub>-ZrO<sub>2</sub> mixed oxide solid solution catalysts prepared via urea hydrolysis. *Appl. Catal. A Gen.* **2002**, *234*, 221–233. [[CrossRef](#)]

38. Roh, H.S.; Potdar, H.S.; Jun, K.W.; Kim, J.W.; Oh, Y.S. Carbon dioxide reforming of methane over Ni incorporated into Ce–ZrO<sub>2</sub> catalysts. *Appl. Catal. A Gen.* **2004**, *276*, 231–239. [[CrossRef](#)]
39. Gregg, S.J.; Sing, K.S.W. Adsorption Surface Area and Porosity. *J. Electrochem. Soc.* **1967**, *114*, 279. [[CrossRef](#)]
40. Menegazzo, F.; Signoreto, M.; Marchese, D.; Pinna, F.; Manzoli, M. Structure–activity relationships of Au/ZrO<sub>2</sub> catalysts for 5-hydroxymethylfurfural oxidative esterification: Effects of zirconia sulphation on gold dispersion, position and shape. *J. Catal.* **2015**, *326*, 1–8. [[CrossRef](#)]
41. Ma, Z.Y.; Yang, C.; Wei, W.; Li, W.H.; Sun, Y.H. Surface properties and CO adsorption on zirconia polymorphs. *J. Mol. Catal. A Chem.* **2005**, *227*, 119–124. [[CrossRef](#)]
42. Guo, R.; Zhou, Y.; Pan, W.; Hong, J.; Zhen, W.; Jin, Q.; Ding, C.; Guo, S. Effect of preparation methods on the performance of CeO<sub>2</sub>/Al<sub>2</sub>O<sub>3</sub> catalysts for selective catalytic reduction of NO with NH<sub>3</sub>. *J. Ind. Eng. Chem.* **2013**, *19*, 2022–2025. [[CrossRef](#)]
43. Khaodee, W.; Tangchupong, N.; Jongsomjit, B.; Praserttham, P.; Assabumrungrat, S. A study on isosynthesis via CO hydrogenation over ZrO<sub>2</sub>–CeO<sub>2</sub> mixed oxide catalysts. *Catal. Commun.* **2009**, *10*, 494–501. [[CrossRef](#)]
44. Harrison, B.; Diwell, A.F.; Hallett, C. Promoting Platinum Metals by Ceria. *Platin. Met. Rev.* **1988**, *32*, 73–83.
45. Eder, D.; Kramer, R. The stoichiometry of hydrogen reduced zirconia and its influence on catalytic activity Part 1: Volumetric and conductivity studies. *Phys. Chem. Chem. Phys.* **2002**, *4*, 795–801. [[CrossRef](#)]
46. Trovarelli, A.; Leitenburg, C.; Dolcetti, G. Design better cerium-based oxidation catalysts. *Chemtech* **1997**, *27*, 32–37.
47. Damyanova, S.; Pawelec, B.; Arishtirova, K.; Huerta, M.V.M.; Fierro, J.L.G. Study of the surface and redox properties of ceria–zirconia oxides. *Appl. Catal. A Gen.* **2008**, *337*, 86–96. [[CrossRef](#)]
48. Li, M.; Wang, X.; Cárdenas-Lizana, F.; Keane, M.A. Effect of support redox character on catalytic performance in the gas phase hydrogenation of benzaldehyde and nitrobenzene over supported gold. *Catal. Today* **2017**, *279*, 19–28. [[CrossRef](#)]
49. Tedsree, K.; Li, T.; Jones, S.; Chan, C.W.; Yu, K.M.; Bagot, P.A.; Marquis, E.A.; Smith, G.D.; Tsang, S.C. Hydrogen production from formic acid decomposition at room temperature using a Ag–Pd core–shell nanocatalyst. *Nat. Nanotechnol.* **2011**, *6*, 302–307. [[CrossRef](#)] [[PubMed](#)]
50. Ojeda, M.; Iglesia, E. Formic Acid Dehydrogenation on Au-Based Catalysts at Near-Ambient Temperatures. *Angew. Chem.* **2009**, *121*, 4894–4897. [[CrossRef](#)]
51. Hengne, A.M.; Kadu, B.S.; Biradar, N.S.; Chikate, R.C.; Rode, C.V. Transfer hydrogenation of biomass-derived levulinic acid to  $\gamma$ -valerolactone over supported Ni catalysts. *RSC Adv.* **2016**, *6*, 59753–59761. [[CrossRef](#)]
52. Li, C.; Xu, G.; Zhai, Y.; Liu, X.; Ma, Y.; Zhang, Y. Hydrogenation of biomass-derived ethyl levulinate into  $\gamma$ -valerolactone by activated carbon supported bimetallic Ni and Fe catalysts. *Fuel* **2017**, *203*, 23–31. [[CrossRef](#)]
53. Wachała, M.; Grams, J.; Kwapiński, W.; Ruppert, A.M. Influence of ZrO<sub>2</sub> on catalytic performance of Ru catalyst in hydrolytic hydrogenation of cellulose towards  $\gamma$ -valerolactone. *Int. J. Hydrogen Energy* **2016**, *41*, 8688–8695. [[CrossRef](#)]
54. Wang, N.; Chua, W.; Zhang, T.; Zhao, X. Manganese promoting effects on the Co–Ce–Zr–O<sub>x</sub> nano catalysts for methane dry reforming with carbon dioxide to hydrogen and carbon monoxide. *Chem. Eng. J.* **2011**, *170*, 457–463. [[CrossRef](#)]
55. Oemar, U.; Hidajat, K.; Kawi, S. Pd–Ni catalyst over spherical nanostructured Y<sub>2</sub>O<sub>3</sub> support for oxy–CO<sub>2</sub> reforming of methane: Role of surface oxygen mobility. *Int. J. Hydrogen Energy* **2015**, *40*, 12227–12238. [[CrossRef](#)]
56. He, J.; Li, H.; Lu, Y.; Liu, Y.; Wu, Z.; Hu, D.; Yang, S. Cascade catalytic transfer hydrogenation–cyclization of ethyl levulinate to  $\gamma$ -valerolactone with Al–Zr mixed oxides. *Appl. Catal. A Gen.* **2016**, *510*, 11–19. [[CrossRef](#)]
57. Li, M.; Collado, L.; Cárdenas-Lizana, F.; Keane, M.A. Role of Support Oxygen Vacancies in the Gas Phase Hydrogenation of Furfural over Gold. *Catal. Lett.* **2018**, *148*, 90–96. [[CrossRef](#)]
58. Bond, G.C. The origins of particle size effects in heterogeneous catalysis. *Surf. Sci.* **1985**, *156*, 966–981. [[CrossRef](#)]

